AIAA JOURNAL
Vol. 45, No. 11, November 2007

Correction Method for Particle Velocimetry Data Based on the Stokes Drag Law

Shunsuke Koike,* Hidemi Takahashi,† Koichi Tanaka,† Mitsutomo Hirota,‡
Kenichi Takita,§ and Goro Masuya¶
Tohoku University, Sendai 980-8579, Japan

DOI: 10.2514/1.30962

A correction method based on the Stokes drag law was developed for flow velocimetry using tracer particles. The present method can be used to calculate the corrected velocity from the measured velocity and its spatial gradient without the need to solve the whole flowfield. Velocity measurement was conducted for sonic transverse injection into Mach 1.8 flow using particle image velocimetry. The correction method was applied to the velocity field obtained from the particle image velocimetry data. The corrected data showed the positions and shapes of the shock waves in the measurement region more clearly. The corrected peak velocity downstream of the shock waves became closer to the theoretical values. The jet streamlines calculated from the corrected and original particle image velocimetry data were compared. The streamlines from the corrected data went lower than those from the original data.

Nomenclature

a	=	sonic speed
C_d	=	drag coefficient of the particle
d_J	=	diameter of the injection hole
d_p	=	diameter of the particle
F	=	correction function
Kn	=	Knudsen number
M	=	Mach number
R	=	gas constant
Re	=	Reynolds number
Rq	=	dynamic pressure ratio
S	=	constant in the Sutherland equation
T	=	static temperature
T_s	=	standard temperature in the Sutherland equation
T_0	=	total temperature
U	=	magnitude of the velocity vector
$\boldsymbol{u}$	=	velocity vector
u	=	streamwise velocity component or component of the velocity vector
v	=	spanwise velocity component
w	=	transverse velocity component
x	=	streamwise coordinate or component of the positional vector
x_{sw}	=	distance from a normal shock wave
y	=	spanwise coordinate
z	=	transverse coordinate
α	=	correction parameter
β_{pi}	=	acceleration component of tracer particles in correction equations for steady flow
γ	=	specific heat ratio
λ	=	mean free path of the molecules
μ_s	=	viscosity coefficient at standard temperature in the Sutherland equation
ρ	=	density

Subscripts

f	=	fluid
fp	=	relative value of the fluid and particle
i, j	=	subscript for the coordinate
J	=	jet
p	=	particle
1	=	weak correction
2	=	strong correction
∞	=	main flow

Received 12 March 2007; accepted for publication 18 July 2007.

*Graduate Student, Department of Aerospace Engineering, JSPS Research Fellow. Student Member AIAA.
†Graduate Student, Department of Aerospace Engineering.
‡Research Associate, Department of Aerospace Engineering.
§Associate Professor, Department of Aerospace Engineering. Member AIAA.
¶Professor, Department of Aerospace Engineering. Senior Member AIAA.

I. Introduction

TECHNIQUES for measuring the velocity of supersonic flows are very important in developing supersonic and hypersonic vehicles and scramjet engines. In recent years, velocity measurement techniques using tracer particles such as laser Doppler velocimetry (LDV), planar Doppler velocimetry (PDV), particle image velocimetry (PIV), particle tracking velocimetry (PTV), and so on, have become very popular, and these techniques are used for supersonic flowfields [1–12].

The basic assumption of velocimetry using tracer particles is that the velocity of the tracer particles is the same as that of the fluid. This assumption is almost valid for incompressible low-speed flows. However, it is often invalid in supersonic flows. In supersonic flows, shock waves appear that produce discontinuous changes in the fluid velocity across them, and tracer particles cannot follow such sudden changes of the fluid velocity. An essentially similar kind of particle response delay occurs in a strong expansion fan and in a vortex core in which the velocity gradient is very high. Thus, the velocity of the particles is not the same as that of the fluid in such regions. These differences produce large errors in the velocity measurement, and it is generally difficult to estimate the magnitude of these errors. Therefore, the response delay of the tracer particles is one of the most serious problems in supersonic velocimetry using the particles.

Several measures have been considered for the problem of the tracer particle response delay. One of these is to improve the performance of the tracer. Urban and Mungal [8], Watanabe and Mungal [9], and Scarano and van Oudheusden [10] used TiO_2 particles for which the diameters were less than or equal to 0.5 μm for PIV. Clancy et al. [5], Elliot et al. [6], and Thurow et al. [7] used ice and condensed acetone particles for which the diameters were less than 0.5 μm for PDV. They measured the supersonic flow with smaller errors. A better way is to use a molecular tracer. Donohue et al. [13] and Donohue and McDaniel [14] successfully measured the complicated supersonic velocity field around the injector and behind the backstep using an iodine tracer. Miles et al. [15] and

Danehy et al. [16] also measured a very simple hypersonic and supersonic velocity field using molecular-tagging velocimetry.

However, these techniques have their own disadvantages. For example, because most small particles for PIV (such as TiO_2) are solid particles, their high-speed impacts sometimes damage the wind-tunnel facility and the models. Moreover, high-power lasers and very sensitive CCD cameras are required to obtain good images of the scattered light from the smaller particles. It is also considered that the damage to a wind tunnel due to I_2 is more severe than that from smaller solid particles. Ice and condensed alcohol particles are better for the damage to the wind tunnel and models. However, their uses are limited by the flow conditions. For these reasons, the improvement of tracer particle performance is limited by the conditions at the wind-tunnel facility, the performance of the measurement systems, and the flow conditions. Although molecular-tagging velocimetry is a desirable technique for hypersonic and supersonic velocimetry, this technique is not practical for the complicated supersonic flowfields at the present.

Another method is a correction for the measured data. If we could correct the response delays of the tracer particles, we could evaluate the flowfield more accurately. A comparison between the original and the corrected data would be useful in identifying regions in which the influence of the response delay of the tracer particles is negligibly small. Furthermore, it may be useful for uncertainty analysis.

The present study adopts the second approach. A method for correcting velocity data measured with tracer particles has been developed and proposed, and numerical validations of this correction method have been conducted. The velocity field of a transverse injection into a Mach 1.8 flow was measured with PIV, and our correction method was applied to these data. The streamlines obtained from the original and corrected data were then compared with the jet trajectory visualized using planar laser-induced fluorescence (PLIF).

II. Theory of the Correction Method

Strictly speaking, the velocity measured with velocimetry using tracer particles is that of the particles. In the present study, the velocity measured with PIV is denoted as the velocity of the particles, $\boldsymbol{u}_p$, and is distinguished from the velocity of the fluid, $\boldsymbol{u}_f$. We will develop a correction method for the case in which the velocity, diameter, and the density of the tracer particles are known.

Generally, the motion of a particle in a fluid can be expressed by the Basset–Bousinesq–Oseen equation [17], which includes terms for the drag that depend on the particle velocity relative to the fluid, the pressure gradient, the added mass, and the nonsteady motion. In a compressible flow, however, in which the density of the particle is much higher than that of the fluid (namely, gas), the drag due to the velocity difference between the fluid and the particle becomes the main part of the total force acting on the particle. Hence, the other terms are neglected [17–19]. In addition, if the flowfield is steady, the equation of motion for the particle can be expressed by Eqs. (1) and (2).

$$u_{pj}\frac{\partial u_{pi}}{\partial x_j} = \frac{3}{4}C_d\frac{\rho_f}{\rho_p}\frac{1}{d_p}|\boldsymbol{u}_{fp}|(u_{fi}-u_{pi}) \tag{1}$$

$$\boldsymbol{u}_{fp} = \boldsymbol{u}_f - \boldsymbol{u}_p \tag{2}$$

Hereafter, Cartesian coordinates are used. The variables u_{fi} and u_{pi} are components of the velocity vectors $\boldsymbol{u}_f$ and $\boldsymbol{u}_p$, respectively. Einstein summation convention is also used for the terms that include subscripts i and j. The left-hand side of Eq. (1) is the acceleration term for steady flow, and the right-hand side is the force acting on the particle divided by the particle mass. Parameters α and β_{pi}, defined by Eqs. (3) and (4), are introduced to simplify the equations.

$$\frac{1}{\alpha} \equiv \frac{3}{4}C_d\frac{\rho_f}{\rho_p}\frac{1}{d_p}|\boldsymbol{u}_{fp}| \tag{3}$$

$$\beta_{pi} \equiv u_{pj}\frac{\partial u_{pi}}{\partial x_j} \tag{4}$$

Using α and β_{pi}, the velocity component of the fluid can then be expressed by Eq. (5).

$$u_{fi} = u_{pi} + \alpha\beta_{pi} \tag{5}$$

where u_{pi} and β_{pi} are known. However, α is a function of the fluid velocity. Therefore, α has to be calculated to obtain the velocity of the fluid, u_{fi}, as mentioned later.

Generally, the drag coefficient C_d is a function of the relative Reynolds number $Re_{fp}(=\rho_f|\boldsymbol{u}_{fp}|d_p/\mu_f)$; the relative Mach number $M_{fp}(=|\boldsymbol{u}_{fp}|/a_f)$; and the Knudsen number $Kn(=\lambda/d_p)$, which is a function of the relative Mach and Reynolds numbers [20]. However, if the relative Reynolds number Re_{fp} is less than unity and the relative Mach number M_{fp} is almost zero, the Knudsen number Kn become almost zero and the drag coefficient C_d can be expressed by the Stokes drag coefficient $C_d = 24/Re_{fp}$. Thus, the density of the fluid, ρ_f, can be canceled in Eqs. (1) and (3) and then Eq. (6) can be obtained.

$$\alpha = \frac{d_p^2\rho_p}{18\mu_f} \tag{6}$$

It should be noted that if other drag coefficients that cover the wider range of Re_{fp}, M_{fp}, and Kn are used, then other physical properties, such as the density or static pressure of the flowfield, will be needed to calculate the drag coefficient because the density of the fluid, ρ_f, in the relative Reynolds number Re_{fp} cannot be canceled.

If the total temperature is known throughout the flowfield, the static temperature can be obtained as the function of α, and the viscosity coefficient can be calculated as a function of the static temperature. If the Sutherland equation is used to obtain the viscosity coefficient, α can be calculated from the following equations.

$$\alpha = \frac{d_p^2\rho_p T_s^{\frac{3}{2}}}{18(T_s+S)\mu_s}\left\{T_{0f} - \frac{\gamma-1}{2\gamma R}|\boldsymbol{u}_\mathbf{f}|^2\right\}^{\frac{-3}{2}}\left\{T_{0f} + S - \frac{\gamma-1}{2\gamma R}|\boldsymbol{u}_\mathbf{f}|^2\right\} \tag{7}$$

$$|\boldsymbol{u}_\mathbf{f}|^2 = \beta_{pi}\beta_{pi}\alpha^2 + 2\beta_{pi}u_{pi}\alpha + u_{pi}u_{pi} \tag{8}$$

The constants in the Sutherland equation for air are 17.16×10^{-6} Ns/m^2 for μ_s, 273.2 K for T_s, and 111 K for S. If the flowfield is three-dimensional, three components of the velocity vectors of the particles are needed for use in Eqs. (5) and (8) to make the correction. With α obtained from Eqs. (7) and (8), the velocity of the fluid can be calculated from Eq. (5). It is worth noting that the flow velocity can be calculated from the local values of the particle velocity components and its spatial gradients without the need to solve the whole flowfield.

It is important to investigate the number of solutions for Eq. (7). Here, a function F is defined as the right-hand side of Eq. (7). The first and second derivatives of the function F are given by the following equations.

$$\frac{dF}{d\alpha} = \frac{\rho_p d_p^2 T_s^{\frac{3}{2}}(\gamma-1)}{36\mu_s(T_s+S)\gamma R}\left(\frac{T_f+3S}{T_f^{\frac{5}{2}}}\right)(\beta_{pi}\beta_{pi}\alpha + \beta_{pi}u_{pi}) \tag{9}$$

$$\frac{d^2F}{d\alpha^2} = \frac{\rho_p d_p^2 T_s^{\frac{3}{2}}(\gamma-1)}{36\mu_s(T_s+S)\gamma R}\left\{\beta_{pi}\beta_{pi}\left(T_f^{\frac{-3}{2}} + 3ST_f^{\frac{-5}{2}}\right) + \frac{3(\gamma-1)}{4\gamma R}(\beta_{pi}\beta_{pi}\alpha + \beta_{pi}u_{pi})^2\left(T_f^{\frac{-5}{2}} + 5ST_f^{\frac{-7}{2}}\right)\right\} \tag{10}$$

Because the static temperature T_f is positive, the second derivative of F from Eq. (10) is also positive. Thus, the function F is a convex-downward curve with no inflection point. This means that the

number of the solutions of Eq. (7) must be two or less. Solutions, if they exist, can be numerically obtained from Eq. (7). At present, it is not possible to select a realistic solution on a theoretical basis. Therefore, numerical validations of the solutions were conducted to identify the appropriate one.

III. Numerical Validation

The correction method described in the previous section was numerically validated for two flows of air with the total temperature of 300 K. These were linearly accelerated and suddenly decelerated flows. First, the particle velocity u_p is calculated from the given velocity distribution of fluid, u_f, using Eq. (1) and assuming the Stokes drag coefficient. Second, the velocity distribution of the fluid is reconstructed from this particle velocity using correction equations (5), (7), and (8). Third, the two solutions from the correction equations u_{f1} and u_{f2} are compared with the given velocity of fluid, u_f.

Figures 1 and 2 show the results of the linearly accelerated flow and suddenly decelerated flow, respectively. In both figures, open circles and open squares represent the given fluid velocity u_f and the particle velocity calculated from Eq. (1), u_p, respectively. Solid triangles show the two correction solutions derived from Eqs. (5), (7), and (8): u_{f1} and u_{f2}. Here, the solutions u_{f1} and u_{f2} correspond to the velocities obtained from the smaller and larger solutions for α. As can be seen from Eq. (5), a smaller α results in a smaller correction and vice versa. Thus, we refer to u_{f1} and u_{f2} as the weak and strong correction solutions.

In both cases, u_{f1} agrees very well with the given fluid velocity u_f over most of the flowfield. The strong correction solution, u_{f2}, agrees with the given velocity only at points at which it exceeds 700 m/s in Fig. 1. Because the stagnation temperature of air is 300 K, a flow velocity of more than 700 m/s corresponds to a static temperature below 60 K. In this condition, actual air condenses and the Sutherland equation is no longer applicable. Thus, in these two example cases, the weak correction solution, u_{f1}, gives the real velocity of the fluid, u_f, when the static temperature is higher than the condensation point and the Sutherland equation is valid. We also checked several cases involving other one-dimensional flows and found that the given velocity could be reproduced by the weak correction solution, u_{f1}, as long as the flow satisfied the conditions mentioned earlier.

These numerical simulations validated this method as suitable for obtaining the real velocity of a fluid, u_f, from the particle velocity u_p, assuming that the weak correction solution, u_{f1}, is selected. Thus, we will hereafter deal with the weak solution, u_{f1}, as the real corrected velocity of the fluid.

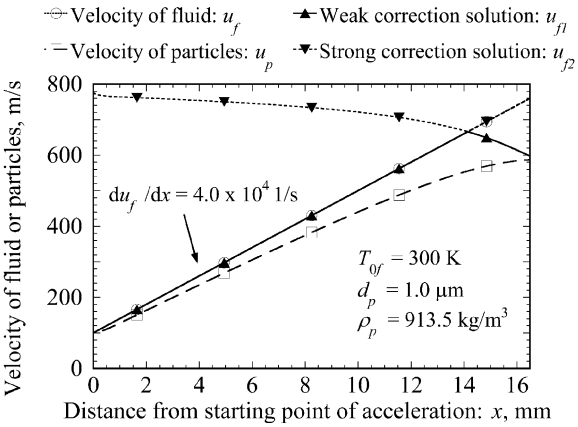

Fig. 1 Numerical validation for acceleration flow.

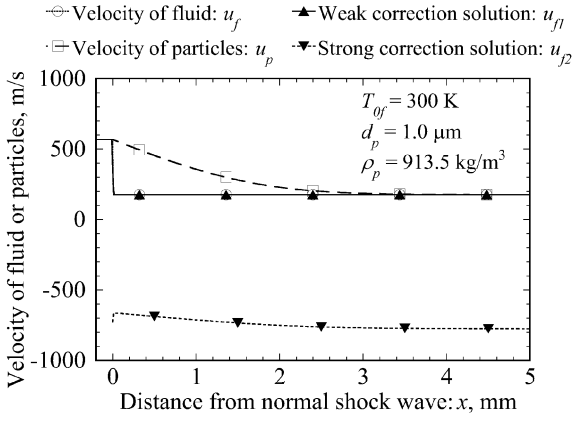

Fig. 2 Numerical validation for a normal shock wave.

IV. Experiment Setup and Conditions

Two experiments were conducted for the present research. One was a transverse injection test and the other was a preliminary experiment for evaluating the tracer particle diameter. The experiment setups for both tests, as well as the PIV system, are discussed in this section.

A. Test Facility for the Transverse Injection Test

Figure 3 schematically diagrams the experiment apparatus for the transverse injection test. A suction-type supersonic wind tunnel was used. Unheated atmospheric air was inhaled into a vacuum tank through a two-dimensional contoured nozzle and a test section. The tank had a volume of 8 m^3 and was evacuated to about 5 kPa before each run. A seeding chamber was placed at the entrance of the nozzle to supply tracer particles into the air for the PIV.

The injectant was pressurized air fed from an air tank. The pressurized air was supplied to the mist generator and produced the tracer particles. One line from the mist generator fed tracer particles to the seeding chamber and the other line supplied the injectant air and particles to an injector attached on one of the walls of the test section.

The test section had a 30-mm-square cross section and was 330 mm long. The walls of the test section were made of clear acrylic resin, except for the wall on which the injector was attached. There was a single injection hole, for which the diameter was 2.5 mm. The center of the injection hole was located 135 mm downstream from the entrance to the test section, on the centerline of the wall. The wall of the injector was painted black to reduce the influence of reflected light on the PIV.

A schematic diagram of the transverse injection flowfield is presented in Fig. 4. The nominal Mach number of the airstream was 1.8. Total temperature of the injectant and the mainstream was atmospheric temperature (283.65 K). Total pressure of the injectant was 186 kPa. The jet-to-mainstream dynamic pressure ratio Rq was 1.8 ± 0.1, assuming an isentropic flow and the sonic injection. The boundary-layer thickness upstream of the injection hole was about 5 mm from the velocity distribution measured by PIV. In the present study, the Cartesian coordinates in Fig. 4 are used to indicate the results. Streamwise, spanwise, and transverse directions correspond to x, y, and z.

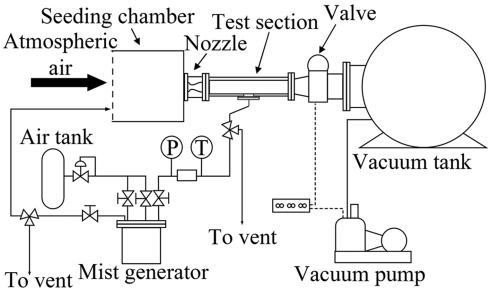

Fig. 3 Schematic of the experimental facility.

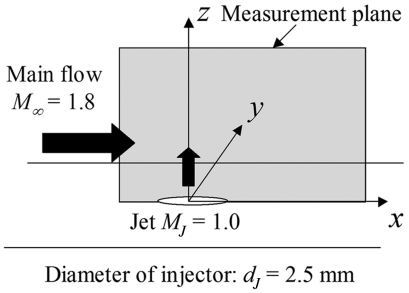

Fig. 4 Schematic of the measurement region and coordinate.

B. Test Facility for the Preliminary Experiment

An objective of the preliminary experiment using a normal shock wave was to estimate the diameter of the tracer particles used in the transverse injection test. Therefore, it is better to estimate the particle diameter under conditions similar to those in the transverse injection test.

The test facility for the preliminary experiment was almost the same as that used for the transverse injection test, but without the injector. The supply system for the tracer particles was the same as that for the mainstream tracer particles in the transverse injection test. Although it would have been better to use the same nozzle and test section used in the transverse injection test, they were changed to produce a single normal shock wave. A pseudo shock wave (PSW) appears due to the interaction between the boundary layer and the shock wave if the length of the test section is sufficiently long and the Mach number of the main stream is sufficiently high. The nominal Mach number of the nozzle for the preliminary test was 1.5, and the length of the test section was 100 mm. The cross section of the test section was the same as that in the transverse injection test. The backpressure in the test section was adjusted using a butterfly valve attached at the exit of the test section, and a single normal shock wave was produced. Unfortunately, a stable single normal shock wave could not be produced in this experiment. Two shock waves often appeared, as mentioned later.

C. PIV

Velocity measurements were conducted using PIV on the x–z plane at $y = 0$ mm for both the transverse injection test and the preliminary experiment. The PIV system is the same as that in our previous research [11]. The measurement was conducted in the double-frame, single-exposure mode of the PIV system. A double-pulsed Nd:YAG laser (532 nm, 12 mJ/pulse, with a pulse duration of 5–7 ns) was used as a light source. A mirror and two cylindrical lenses were used to produce a laser sheet about 0.5 mm thick and 50 mm wide. Scattered light from the particles was recorded with a CCD camera (1280 × 1024 pixels). The resolution of the recording for the transverse injection test was 44.5 μm/pixel; that for the preliminary experiment was 32.6 μm/pixel. The laser and the CCD camera were synchronized with a synchronizer. The separation time of successive laser pulses was 400 ns. Image data were transferred to a PC for processing to calculate the velocity vectors using the cross-correlation method with an analyzing program (TSI, Inc., INSIGHT3.32). The interrogation area was 32 × 32 pixels, and the grid interval was 0.5 mm.

The methodology for the eliminating error vectors was the same as that used in our previous research [11] for the transverse injection test. This methodology is used for averaged data and is not applicable to instantaneous data. As mentioned previously, the shock wave was unstable, and so we needed instantaneous velocity data for the preliminary experiment. Furthermore, only velocity data on the centerline of the duct was used in the preliminary experiment. Hence, we made the following elimination rules for the preliminary experiment. First, if the streamwise velocity component, u, is less than 50 m/s or greater than 600 m/s, or if the absolute value of the transverse velocity component, w, is greater than 100 m/s, the velocity vector is eliminated. Second, spatial averages of u and w at a certain point and at eight points around the point are calculated and their standard deviations are obtained. Third, if the difference between u or w on the principal point and the nine-point average exceed twice the standard deviation, the velocity vector for that point is eliminated. In the first step of the preceding elimination process, the velocity vectors in the boundary layer were removed. Because only velocity data for the centerline of the duct were used in the preliminary experiment and because it was very important to completely eliminate suspicious vectors, this severe elimination was conducted as the first step.

The tracer particles for the PIV were droplets of dioctyl sebacate (density 913.5 kg/m^3) produced with Laskin nozzles [21,22] in a mist generator. The diameter of the tracer particles was measured to be about 1.0 μm by Kitamura [23] using the gravitational sedimentation method. However, in our previous research [11], the diameter of the tracer particles was estimated at about 2.0 μm, based on the response of particles in the downstream region of the Mach disk produced in an underexpanded jet ejected from a conical nozzle. In that research, the particle diameter was estimated by assuming a single sudden velocity reduction from the highest to the lowest velocity measured. However, several weak shock waves could be seen around the Mach disk in the schlieren photos. Therefore, it was considered that the difference in the particle-diameter values obtained with the two experiments was mainly due to the difference between the actual flow structure downstream of the Mach disk and the assumed ideal conditions in the estimation. Hence, in the present research, the preliminary experiment was conducted with a better-defined normal shock wave to estimate the diameter of the tracer particles more accurately.

V. Results and Discussion

A. Preliminary Experiment

Figure 5 presents schlieren photographs of the shock waves in the preliminary experiment. Figure 5a shows a normal shock wave without tracer particles, and Figs. 5b and 5c show shock waves with particles. A region shown in these photographs is about 20 mm downstream from the entrance of the test section.

In the present experiment, a single normal shock wave was obtained only at the position shown in Fig. 5. Furthermore, because

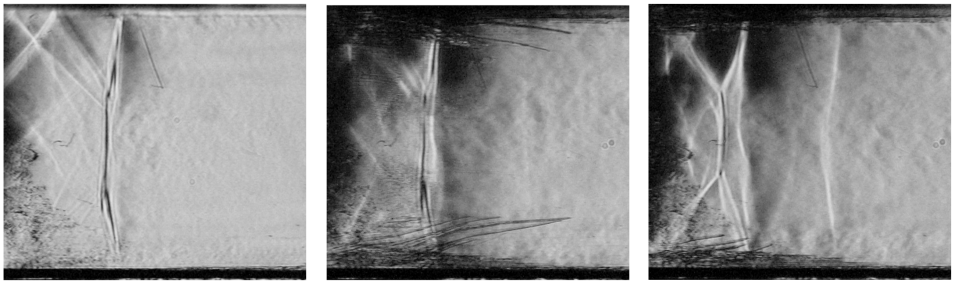

a) Without particles **b) With particles (single normal shock wave)** **c) With particles (PSW)**

Fig. 5 Schlieren photograph.

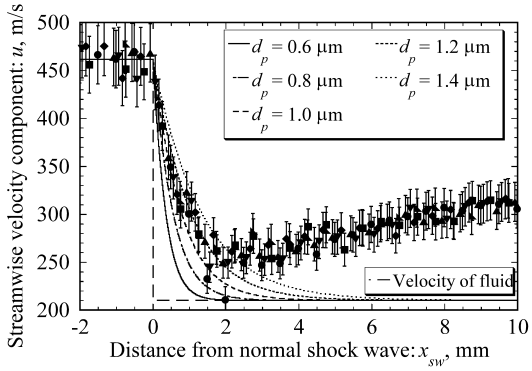

Fig. 6 Velocity in the downstream region of the normal shock wave.

of small fluctuations in the particle supply system, the shock wave vibrated. As a result, there were the cases in which the single normal shock wave or two or more shock waves (PSW) appeared during the single run.

Although it is not clear in Fig. 5, fan-shaped dark regions expanded from the region of the shock-wave/boundary-layer interaction to the centerline of the duct. These fan-shaped regions were expansion waves. Thus, the velocity on the centerline of the duct increased again in the downstream region of the normal shock wave.

As mentioned earlier, we do not have much velocity data for the ideal normal shock wave. Figure 6 show the velocity data for an ideal normal shock wave and the response curve of the particles calculated from Eq. (1), assuming a normal shock wave and the Henderson drag coefficient [20], which can be applied over a much wider range of Reynolds and Mach numbers. Figure 6 presents streamwise velocity component data along the centerline of the duct. The error bars were estimated from the average difference between the velocity measured with a pitot/static pressure tube and with PIV in our previous research [1]. Taking the vibration of the normal shock wave into account, the velocity at the first point following the decelerating point was fitted to the response curve calculated from Eq. (1), assuming that the particle diameter was 1.0 μm, the value measured with the gravitational sedimentation method.

Because of the expansion waves mentioned earlier, the velocity gently increased from about $x_{\mathrm{sw}} = 2$ mm. Because the response curve was calculated assuming only a normal shock wave, the comparison between the measured velocity and the calculated response curves should be made in the region of x_{sw} less than 2 mm. All measured data are from the region between the response curves of $d_p = 0.6$ and 1.4 μm. From this result, we concluded that the diameter of the tracer particles in the test section was almost the same as that estimated by means of the gravitational sedimentation method: 1.0 μm. Therefore, a particle diameter of 1.0 μm was used for the correction.

B. Transverse Injection Test

Figure 7 presents the distributions of the streamwise and the transverse averaged velocity components, u_p and w_p, measured with PIV in the $y = 0$ mm plane. These distributions of the averaged velocity components were obtained from 210 pairs of pictures with the elimination process of error vectors [11]. This flowfield included the following (letters in parentheses correspond to Fig. 7): a transverse jet (A), a separation shock wave (B), a bow shock wave (C), a reflection shock wave from the upper wall (D), expansion waves from the interaction point of the bow shock wave and boundary layer (E), and a reattachment shock wave from the lower wall (F). The magnitude of w_p was high in the region near the lower wall (G). This high magnitude of w_p represents the upward velocity induced by streamwise vortices due to the transverse jet.

The angle of the bow shock wave at $z = 15$ mm was about 45 deg, and certain physical properties can be calculated from this angle. Unfortunately, the relative Reynolds number was 4, and the relative Mach number was 0.4 in the region just behind the bow shock wave. Generally, the Stokes drag law is applicable under conditions in which the relative Reynolds number is less than unity and the relative Mach number is negligibly small. Hence, these values somewhat exceeded the applicable range of the Stokes drag law, though they were not very far from the range. In addition, because such regions were very limited in size, the Stokes drag coefficient could be applied to the majority of the flowfield. Therefore, the present correction method gave a good corrected velocity field, as described later.

Figure 8 shows the distribution of the weak correction solutions, u_{f1} and w_{f1}, and Fig. 9 shows that of the strong correction solutions, u_{f2} and w_{f2}. These solutions were calculated assuming a spanwise velocity component v of zero due to the symmetry of the flowfield. The blank regions in the figures are regions in which the correction equations do not have a solution. At these points, the contour lines of the original velocity measured with PIV were not sufficiently smooth. Therefore, the lack of solution was mainly due to the errors of the original data. From a comparison between Figs. 7–9, it is clear that the weak correction solution was the suitable one for the correction equations. Although the contour lines of the corrected data in Figs. 8a and 8b were not smooth, due to the error in the numerical differentials, the contour lines just behind the shock waves were concentrated more closely than in the original distribution. The position and shape of the shock waves were clearer in the corrected contours than in the original ones, particularly for the bow shock wave and the reflected shock wave.

It is interesting to compare the corrected velocity in the region downstream of the bow shock wave with the theoretical value, calculated assuming a shock wave angle of 45 deg. Figure 10 shows the streamwise and transverse velocity components on the line of $z = 15$ mm. Solid (open) circles represent the original (corrected) data for the streamwise velocity component, u, and solid (open) squares represent those of the transverse component, w. Solid and broken straight lines show the theoretical values of u and w just behind the oblique shock wave.

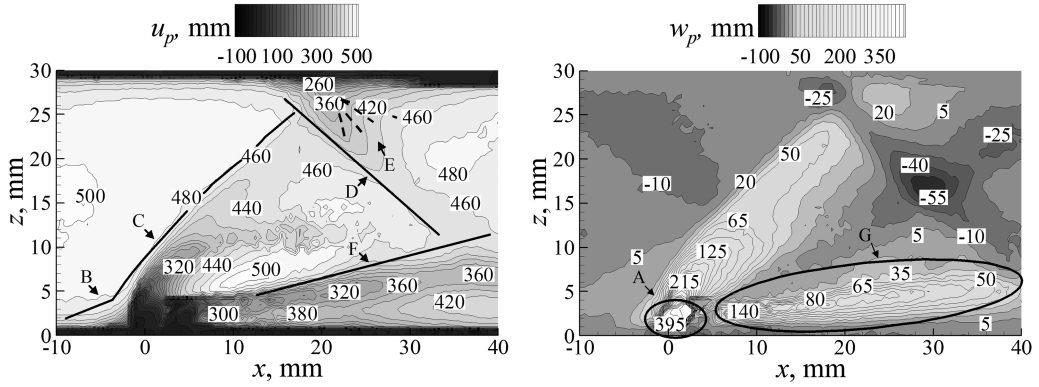

a) Streamwise velocity component **b) Transverse velocity component**

Fig. 7 Contour of the velocity component measured with PIV.

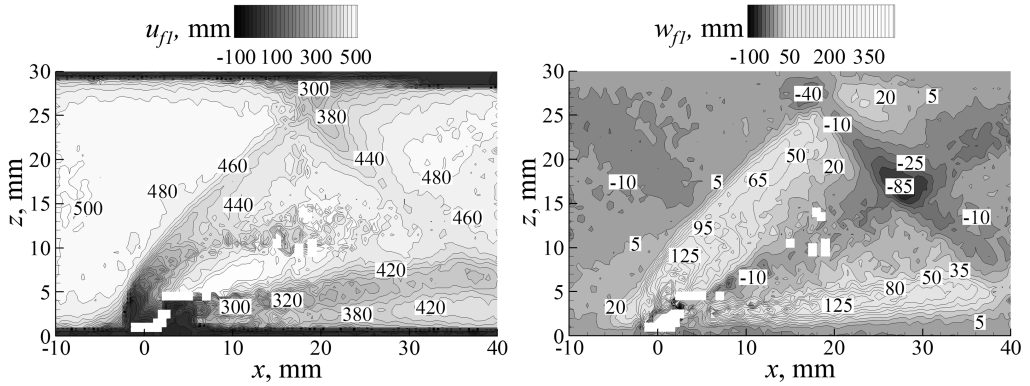

a) Streamwise velocity component b) Transverse velocity component

Fig. 8 Contour of the corrected velocity (weak correction solution).

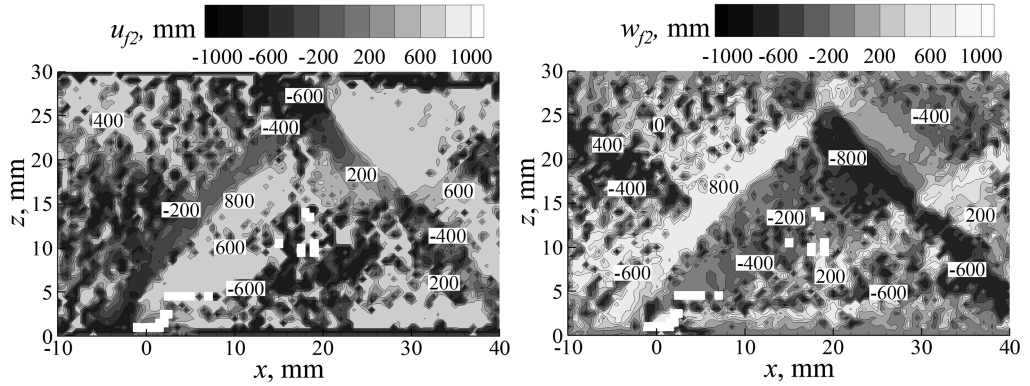

a) Streamwise velocity component b) Transverse velocity component

Fig. 9 Contour of the corrected velocity (strong correction solution).

In Fig. 10, the minimum value of u_{f1} and the maximum value of w_{f1} were closer to the theoretical lines than were those of the original data. The position at which the corrected velocity components had their minimum and maximum values approached closer to the starting point of the velocity change. Because this starting point was the position of the bow shock wave, the corrected data showed a more accurate velocity distribution.

Figure 11 presents the distribution of the difference between the original and corrected magnitude of the velocity vector normalized by the velocity of the main stream on the $y = 0$ mm plane. The difference took a large negative value in the region downstream of the bow shock wave near the injector and a large positive value in the region of the concentrated expansion waves. In contrast, the difference was small in a region upstream of the injection hole and near the lower wall at $x > 20$ mm. This means that the influence of the response delay of the particles on the measured velocity was small in those regions. Therefore, the original velocity data measured with PIV were reliable in those regions.

Figure 12 compares between the trajectory of the peak in the acetone PLIF signal intensity and Mie-scattered light signal intensity [24] and the jet streamlines calculated from the original and corrected velocity data. The dynamic pressure ratios Rq were 1.7 and 1.9 for the PLIF and Mie-scattered light visualization. These values were slightly lower and higher than the dynamic pressure ratio of the present PIV experiment, which was 1.8. Only the jet was supplied with either acetone vapor for PLIF or the tracer particles for Mie-scattered light visualization. The tracer particles were the same as those in our PIV [24]. Unfortunately, due to the lack of the corrected

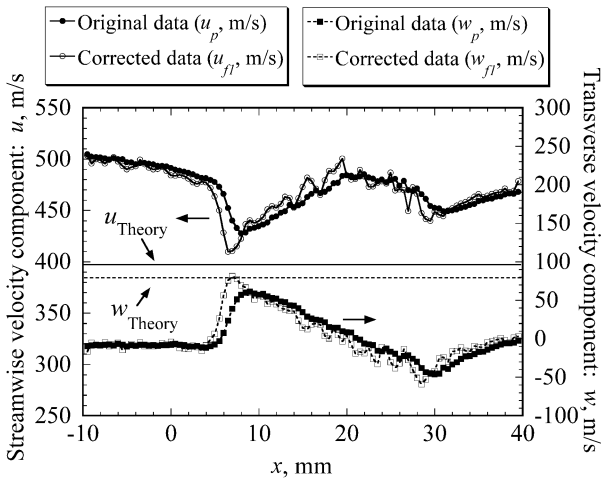

Fig. 10 Velocity component on the centerline of the test section.

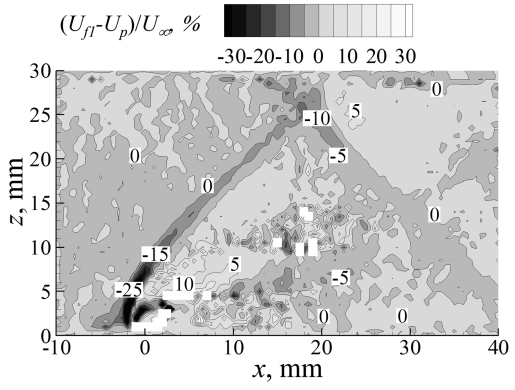

Fig. 11 Difference between the original and corrected data normalized by the velocity of the mainstream.

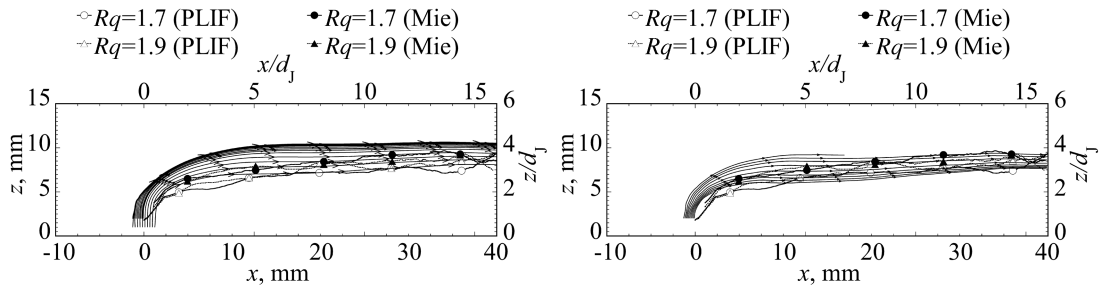

a) Original data **b) Corrected data**

Fig. 12 Comparison between the streamlines and PLIF trajectory.

solutions at the points just above the injection port, only the streamlines starting from the points between $x = -1.25$ and -0.05 mm at $z = 2$ mm were obtained for the corrected data. In the original data, the streamlines started from the same points as in the corrected data, and those starting from $z = 1$ mm and just above the injection hole are shown.

Because acetone PLIF uses a molecular tracer, the peak trajectory of the acetone PLIF signal intensity represents the trajectory of the jet more accurately than does the Mie-scattered light signal intensity. Takahashi et al. [24] compared the peak trajectory of Mie-scattered light with the PLIF trajectory, as shown in Fig. 12. From a comparison of these trajectories, it is obvious that the Mie trajectory went higher than the PLIF trajectory. This difference was mainly caused by the response delay of the tracer particles. In the other words, the response delay of the tracer particles changed the trajectory of the tracer in the jet to the position higher than the real trajectory of the jet. Therefore, if the correction is valid, the corrected streamlines go lower than the original streamlines.

In Fig. 12b, the corrected streamlines went lower than the original ones. This tendency agreed with the prediction from the comparison between the PLIF and the Mie-scattered light trajectories. Hence, our velocity correction method is qualitatively applicable to correct the streamlines.

VI. Conclusions

A correction method based on the Stokes drag law was developed and proposed for the flow velocimetry using tracer particles. An analysis of the correction equations revealed that the number of solutions was two or less. Numerical validation indicated that the solution closer to the particle velocity was the realistic correction.

The diameter of the tracer particles was estimated with a test using a normal shock wave. The result suggested that a tracer particle diameter was about 1 μm, and this value was used in the correction. Velocity measurement was conducted with PIV for a sonic transverse injection into a Mach 1.8 flow, and the correction method was then applied to this PIV data. The corrected data represented the positions and shapes of the shock waves more clearly. The corrected peak velocity downstream of the shock waves was more accurate than the original data. The jet streamlines calculated from the corrected and original PIV data were compared. The streamlines from the corrected data went lower than those from the original data.

Acknowledgments

This work was supported by Research Fellowships of the Japan Society for the Promotion of Science for Young Scientists through grant 17004966. Hiroki Oso and Takashi Iwase supported us for the experiment, and Eijiro Kitamura gave us advice on the correction method. We wish to express our gratitude to them.

References

[1] Herrin, J. L., and Dutton, J. C., "Supersonic Base Flow Experiments in the Near Wake of a Cylindrical Afterbody," *AIAA Journal*, Vol. 32, No. 1, 1994, pp. 77–83.

[2] Santiago, J. G., and Dutton, J. C., "Velocity Measurements of a Jet Injected into a Supersonic Crossflow," *Journal of Propulsion and Power*, Vol. 13, No. 2, 1997, pp. 264–273.

[3] Palko, C. W., and Dutton, J. C., "Velocity Measurements in a Shock-Separated Free Shear Layer," *AIAA Journal*, Vol. 38, No. 7, 2000, pp. 1237–1245.

[4] Smith, M. W., Northam, G. B., and Drummond, J. P., "Application of Absorption Filter Planar Doppler Velocimetry to Sonic and Supersonic Jets," *AIAA Journal*, Vol. 34, No. 3, 1996, pp. 434-441.

[5] Clancy, P. S., Samimy, M., and Erskine, W. R., "Planar Doppler Velocimetry: Three-Component Velocimetry in Supersonic Jets," *AIAA Journal*, Vol. 37, No. 6, 1999, pp. 700–707.

[6] Elliott, G. S., Samimy, M., and Arnette, S. A., "A Molecular Filter Based Velocimetry Technique for High Speed Flows," *Experiments in Fluids*, Vol. 18, Nos. 1–2, Dec. 1994, pp. 107–118. doi:10.1007/BF00209367

[7] Thurow, B. S., Jiang, N., Lempert, W. R., and Samimy, M., "Development of Megahertz-Rate Planar Doppler Velocimetry for High-Speed Flows," *AIAA Journal*, Vol. 43, No. 3, 2005, pp. 500–511.

[8] Urban, W. D., and Mungal, M. G., "Planar Velocity Measurements in Compressible Missing Layers," *Journal of Fluid Mechanics*, Vol. 431, June 2001, pp. 189–222. doi:10.1017/S0022112000003177

[9] Watanabe, S., and Mungal, M. G., "Velocity Fields in Mixing-Enhanced Compressible Shear Layers," *Journal of Fluid Mechanics*, Vol. 522, Jan. 2005, pp. 141–177. doi:10.1017/S0022112004001727

[10] Scarano, F., and van Oudheusden, B. W., "Planar Velocity Measurements of a Two-Dimensional Compressible Wake," *Experiments in Fluids*, Vol. 34, No. 3, 2003, pp. 430–441.

[11] Koike, S., Suzuki, K., Kitamura, E., Hirota, M., Takita, K., and Masuya, G., "Measurement of Vortices and Shock Waves Produced by Ramp and Twin Jets," *Journal of Propulsion and Power*, Vol. 22, No. 5, 2006, pp. 1059–1067.

[12] Nakamura, H., Sato, N., Kobayashi, H., and Masuya, G., "Measurement of Supersonic Flow Field Using Particle Tracking Velocimetry," *21st International Congress on Instrumentation in Aerospace Simulation Facilities, ICIASF'05 Record* [CD-ROM], Inst. of Electrical and Electronics Engineers, Piscataway, NJ2005, pp. 323–328.

[13] Donohue, J. M., McDaniel, J. C., and Haj-Hariri, H., "Experimental and Numerical Study of Swept Ramp Injector into a Supersonic Flowfield," *AIAA Journal*, Vol. 32, No. 9, 1994, pp. 1860–1867.

[14] Donohue, J. M., and McDaniel, J. C., "Computer-Controlled Multiparameter Flowfield Measurements Using Planar Laser-Induced Iodine Fluorescence," *AIAA Journal*, Vol. 34, No. 8, 1996, pp. 1604–1611.

[15] Miles, R. B., Grinstead, J., Kohl, R. H., and Diskin, G., "The RELIEF Flow Tagging Technique and its Application in Engine Testing Facilities and for Helium-Air Mixing Studies," *Measurement Science and Technology*, Vol. 11, No. 9, 2000, pp. 1272–1281. doi:10.1088/0957-0233/11/9/304

[16] Danehy, P. M., O'Byrne, S., Frank, A., Houwing, P., Fox, J. S., and Smith, D. R., "Flow-Tagging Velocimetry for Hypersonic Flows Using Fluorescence of Nitric Oxide," *AIAA Journal*, Vol. 41, No. 2, 2003, pp. 263–271.

[17] Soo, S. L., *Fluid Dynamics of Multiphase Systems*, Blaisdell, Waltham, MA, 1967.

[18] Thomas, P. J., "On the Influence of the Basset History Force on the Motion of a Particle," *Physics of Fluids A*, Vol. 4, No. 9, 1992, pp. 2090–2093. doi:10.1063/1.858379

[19] Thomas, P. J., Bütefisch K. A., and Sauerland, K. H., "On the Motion of Particles in a Fluid Under the Influence of a Large Velocity Gradient," *Experiments in Fluids*, Vol. 14, Nos. 1–2, Dec. 1993, pp. 42–48.

[20] Henderson, C. B., "Drag Coefficients of Sphere in Continuum and Rarefied Flow," *AIAA Journal*, Vol. 14, No. 6, 1976, pp. 707–708.
[21] Melling, A., "Tracer Particles and Seeding for Particle Image Velocimetry," *Measurement Science and Technology*, Vol. 8, No. 12, 1997, pp. 1406–1416. doi:10.1088/0957-0233/8/12/005
[22] Kähler, C. J., Sammler, B., and Kompenhans, J., "Generation and Control of Tracer Particles for Optical Flow Investigations in Air," *Experiments in Fluids*, Vol. 33, No. 6, 2002, pp. 736–742.
[23] Kitamura, E., Matsumoto, M., Koike, S., and Masuya, G., "PIV Measurement of Supersonic Swirling Jet," *Proceedings of the 30th Symposium on Visualization*, Visualization Society of Japan, Tokyo, 2002, pp. 189–192 (in Japanese).
[24] Takahashi, H., Hirota, M., Oso, H., and Masuya, G., "Measurement of Supersonic Injection Flowfield Using Acetone PLIF," *Journal of the Japan Society for Aeronautical and Space Sciences* (to be published) (in Japanese).

R. Lucht
Associate Editor